BJRS
BRAZILIAN JOURNAL OF RADIATION SCIENCES

doi.org/10.15392/2319-0612.2024.2483
2024, 12(3) | 01-20 | e2483
Submitted: 2024-05-02
Accepted: 2024-08-07

Methodology study for determining the half-value layer using the Monte Carlo code PHITS

Soares[a*], R. E.; Lacerda[b], M. A. S.

[a] Departamento de Física, Instituto de Ciências Exatas - Universidade Federal de Minas Gerais (ICEX/UFMG), 31.270-901, Belo Horizonte, Minas Gerais, Brasil.

[b] Laboratório de Calibração de Dosímetros, Centro de Desenvolvimento da Tecnologia Nuclear (CDTN/CNEN), 31.270-901, Belo Horizonte, Minas Gerais, Brasil.

*Correspondence: ronaldeduardos@ufmg.br

Abstract: For most purposes, the quality of a beam can be specified in terms of the half-value layer (HVL), which is the thickness of material required to reduce the air kerma (K_a) to half, at one meter from the source, from a unidirectional beam of infinitesimal width. Just like many other radiological quantities of interest, the HVL can be estimated via simulations employing the Monte Carlo Method (MCM). Among the variety of MCM based codes available, the Particles and Heavy Ions Transport Code System (PHITS) was the one adopted in this study. Primarily, simulations were conducted to determine the X-ray spectra resulting from the interaction of electron beams with different energies with a tungsten anode. Each of these spectra was then defined as a probability distribution for the photon source energies in a second round of simulations, where it was possible to estimate the X-ray beam qualities as specified by the reference literature. At this stage, it was possible to estimate the mean energy of the beam $(\overline{E})$ and the conversion coefficient for air kerma per unit fluence (K_a/Φ) for each of the qualities. The results obtained in this phase were used to define the sources for other groups of simulations, where the air kerma was quantified for each source configuration, for different thicknesses of an aluminum metallic attenuator, which was also done with spectra for the same X-ray beam qualities obtained from a reference catalog. Curve fitting on the scatter of kerma points as a function of attenuation allowed the estimation of the HVL. The results obtained are consistent with the values described in the literature and demonstrate the efficiency of the developed methodology, as well as the use of the code in the evaluated energy range for X-rays.

Keywords: half-value layer, Monte Carlo Method, PHITS.

BJRS
BRAZILIAN JOURNAL OF RADIATION SCIENCES

doi.org/10.15392/2319-0612.2024.2483
2024, 12(3) | 01-20 | e2483
Submitted: 2024-05-02
Accepted: 2024-08-07

Estudo de uma metodologia para determinação da camada semirretudora utilizando o código de Monte Carlo PHITS

Resumo: Para a maioria dos propósitos, a qualidade de um feixe pode ser especificada em termos da camada semirredutora (CSR), que é a espessura de material necessária para reduzir à metade o kerma no ar (K_a), a um metro da fonte, de um feixe unidirecional de largura infinitesimal. Assim como para muitas outras grandezas de interesse radiológico, a CSR pode ser estimada via simulações que empregam Método de Monte Carlo (MMC). Dentre a variedade de códigos que empregam o MMC disponíveis, o Particles and Heavy Ions Transport Code System (PHITS) foi aquele adotado nesse trabalho. Primordialmente, foram realizadas simulações para determinar os espectros de raios-X provenientes da interação de feixes de elétrons com diferentes energias com um anodo de tungstênio. Cada um desses espectros foi, então, definido como distribuição de probabilidades para as energias da fonte de fótons em uma segunda rodada de simulações, em que foi possível estimar os espectros de radiação de diferentes qualidades de campos conforme especificadas pela bibliografia de referência; nessa etapa foi possível estimar a energia média do feixe $(\overline{E})$ e os coeficiente de conversão para kerma no ar por unidade de fluência (K_a/Φ) para cada uma das qualidades. Os resultados obtidos nessa fase foram empregados para a definição das fontes de outros grupos de simulações, em que o kerma no ar foi quantificado, para cada configuração de fonte, para diferentes espessuras de um atenuador metálico de alumínio, o que também foi feito com os espectros para as mesmas qualidades de campos obtidos em um catálogo de referência. Ajustes de curvas sobre a dispersão dos pontos do kerma em função da atenuação possibilitaram estimar a CSR. Os resultados obtidos são consistentes com os valores descritos na bibliografia e evidenciam a eficiência da metodologia desenvolvida, mas também do emprego do código no intervalo de energia avaliado para os raios-X.

Palavras-chave: camada semirredutora, Método de Monte Carlo, PHITS.

SBPR

1. INTRODUCTION

The quality of a filtered X radiation can be characterized in ISO 4037-1 through several parameters such as: the mean energy $(\overline{E})$, its resolution (R_E), and the homogeneity coefficient (h), in addition to the half-value layer (HVL), expressed in millimeters of Aluminum or Copper for low-energy beams. The HVL can be defined, in these circumstances, as the thickness of attenuating material that reduces the air kerma of a unidirectional beam of infinitesimal width to half of its initial value. In practice, this quality is associated with the applied potential difference in the tube, the total filtration to which the beam is subjected, the distance between the focal spot and the target, and the properties of the anode, in terms of composition and angle [1].

In general, a complete specification of X-ray beam quality would require knowledge of the spectrum, so expressing this characteristic strictly in terms of the HVL is a rough approximation. However, for most purposes, this complete specification of fluences for each energy interval is unnecessary, and specifying the quality in terms of the HVL is usually sufficient [2].

The intensity I of a radiation beam, with initial intensity I_0, after passing through an attenuator with linear attenuation coefficient μ, is related to the thickness x of the attenuator according to Eq. 1.

$$I = I_0 e^{-\mu x} \quad (1)$$

In the case where the thickness of the attenuator is equal to the HVL for that material, the kerma, and therefore also the intensity, by definition, is reduced by half. Thus, the relationship between the linear attenuation coefficient μ and the HVL for a given material can be expressed as evident in Eq. 2, which allows the rewriting of Eq. 1 as expressed in Eq. 3 [3].

$$\mu = \frac{\ln(2)}{HVL} \qquad (2)$$

$$I = I_0 e^{-\frac{\ln(2)}{HVL}x} \qquad (3)$$

In the process of measuring the HVL, one must exclude the contribution of all scattered radiation that is not originally present in the beam. This implies the need for good geometry conditions for executing the measurement, as the configuration should minimize the influence of scattering, which can lead to an overestimation of the obtained value [1,4]. The standard procedures to be adopted for the experimental measurement of the HVL are described in ISO 4037-1, in accordance with ICRU Report 10b and the provisions by Ed (1960) [5,6].

Most of the X-ray dosimetry calculations nowadays are based on estimates made via the Monte Carlo Method (MCM). Named in allusion to the capital of the Principality of Monaco, famous for gambling, the technique is based on the generation of uniformly distributed random numbers between 0 and 1, which allows reproducing any probability distribution, applicable to the study of a variety of objects of knowledge from different areas, with emphasis on particles transport. Thus, based on the physical knowledge related to the interaction of radiation with matter, such as known probability density functions for scattering as a function of angle and energy, one can estimate the three-dimensional distribution of particles fluence, as well as the deposited energy, for a modelled geometry and radiation sources with specific characteristics [3]. Compared to deterministic methods, the main advantage of Monte Carlo algorithms for this application lies in their ability to adapt to complex geometries [7].

With the increase in computing power per unit cost over the last five decades, along with the growing availability of powerful software and tools, there has been a significant increase in the number of scientific publications of medical interest that employ these

techniques. Just in "Physics in Medicine and Biology," for example, between 1967, when the first article with the terms "Monte Carlo" in the title or abstract was published, and 2000, there was a doubling in the number of publications employing Monte Carlo based algorithms every 5 years [8].

Currently, there are various computational codes available that employ Monte Carlo Method (MCM) for particles transport [9-13], with the Particles and Heavy Ions Transport Code System (PHITS) [14] being a prominent example. In addition to its agility, free availability, and ease of obtaining a license, PHITS stands out for its well-prepared tutorial, intuitive syntax allowing parameter introduction, and being the first code system applied to heavy ions transport.

The objective of this study is to present a methodology for determining the HVL using the Monte Carlo code PHITS [14].

2. MATERIALS AND METHODS

The simulations were conducted in three successive stages, followed by data analysis to determine the HVL, as schematically outlined in the flowchart and detailed below.

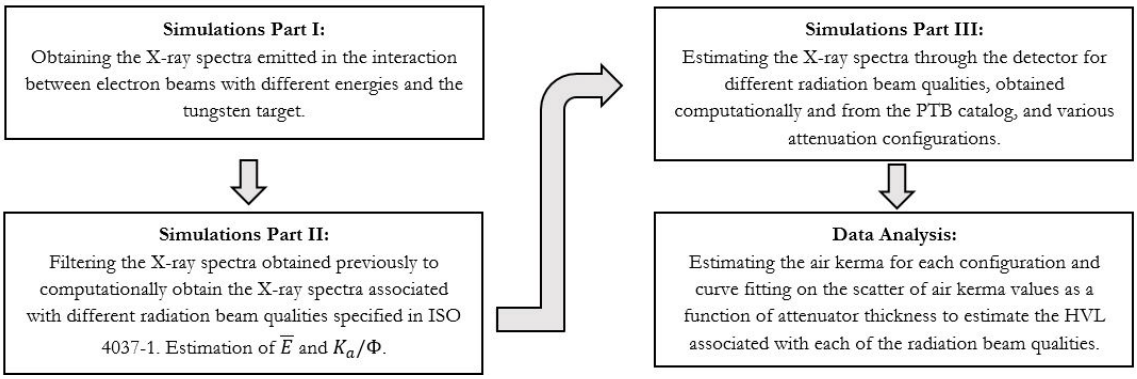

2.1. Obtaining the final computational X-ray spectra for the interaction of monoenergetic electron beams with a tungsten target

Initially, a rotating tungsten anode, with a 20° anode angle, was modelled in vacuum, like that developed by CAMPILLO-RIVERA et al. (2021) [15]. A spherical shell, with a radius of 5 cm, was modelled around it. There is no material between the shell and the anode, representing a vacuum in this context. Then, the interaction of monoaxial and monoenergetic electron beams with rays of approximately 0.027 cm with the anode was simulated, with the spectrum of photons flowing through the surface of the spherical shell quantified using the T-Cross tally, with energy discretization in intervals of 1 keV.

Electron beams with energies of 30 keV, 60 keV, 80 keV, 100 keV, 200 keV, and 300 keV were simulated to obtain the X-ray photons emission spectra for different energies. In all these simulations, the number of histories evaluated was 2.5×10^8. The schematic illustration of the geometry of these simulations, which were performed using PHITS, is shown in Figure 1.

Figure 1 : Schematic illustration of the geometry used in the first phase of simulations, performed using PHITS.

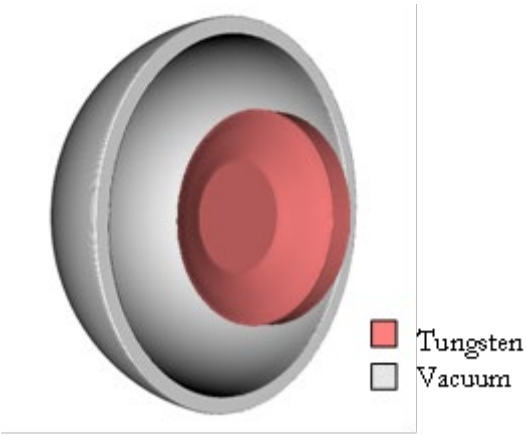

2.2. Obtaining computational X-ray spectra for qualities N30, N60, N80, N100, N200, and N300, and estimating the $\overline{E}$ and the K_a/Φ

The space for these new simulations is delimited by a cylinder with a length of 1.05 m and a radius of 1.05 cm. Near one of its ends, particles sources are defined, in vacuum; however, this time, isotropic photon sources with probability distributions for the energies given by each of the spectra obtained in the previous simulations are defined. Between the region where each of the sources is defined and a spherical detector, defined in dry air, with a radius of 1 cm and located at the opposite end, a 2 mm thick glass layer and a 1 cm thick air layer are interposed; in addition to this air layer, for each of the defined sources, there is a distinct succession of metallic attenuators, according to the specifications of ISO 4037-1 [1] for the different qualities of X-ray beam, as listed in Table 1.

Table 1 : Specifications for the thicknesses and materials of the attenuators used in obtaining the respective qualities specified in ISO 4037-1 [1].

	Total filtration			
ISO 4037-1 quality	**mmAl**	**mmCu**	**mmSn**	**mmPb**
N30	4.0	-	-	-
N60	4.0	0.6	-	-
N80	4.0	2.0	-	-
N100	4.0	5.0	-	-
N200	4.0	2.0	3.0	1.0
N300	4.0	-	3.0	5.0

In all these simulations, performed using PHITS, in turn, the radiation spectrum through the detector was quantified using the T-Track tally, once again with energy discretized in intervals of 1 keV. This narrow beam configuration was adopted to mitigate the contribution of photons backscattered by the attenuators to the spectrum, like what was done by De Jesus Teixeira et al. (2019) [16]. The number of simulated histories now, for each

of the configurations, was 5×10^{10}. Figure 2 shows a scale-out sketch of the geometry used for the simulation through which the spectrum for quality N200 was obtained and which is like that defined for obtaining those associated with the other qualities.

Figure 2 : Scale-out sketch of the geometry used for estimating the spectrum of quality N200, according to the specifications of ISO 4037-1 [1]. The defined materials were vacuum, glass, dry air, lead, aluminum, tin and copper.

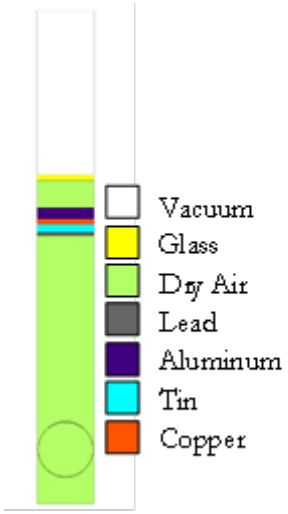

With the estimated spectra for each beam quality, one can calculate the value of the mean energy for each of them and, through linear interpolation of the values described in the literature for monoenergetic photons [17], also the conversion coefficients for air kerma per unit fluence. All calculations described in this article, as well as curve fittings, were performed using algorithms written in R (version 4.4.0) [18].

For comparative purposes, the detailed procedures below for estimating the HVL were also carried out with the spectra from the PTB catalog for the respective qualities [19].

2.3. Estimation of the X-ray spectra through the detector for different beams and attenuation configurations

For each radiation beam quality, with the spectra obtained via computational simulation, sources of photons were defined in the same region delimited previously, but now filled with dry air, except for the small segment where an aluminum attenuator, of

variable thickness, is placed. These sources now have probability distributions for energies according to each of the spectra obtained computationally for the qualities and also from the spectra obtained from the PTB catalog [19]. For each of the computational spectra and catalog spectra, a simulation was conducted without the interposition of an attenuator and 7 others with the interposition of attenuators of different thicknesses. Using PHITS, once again, the radiation spectra through the detector were quantified with the T-Track tally with energy discretized in intervals of 1 keV, and the number of simulated histories in each configuration was 5×10^{10}.

In this stage of the work, 96 simulations were performed, divided into 12 groups, each with a radiation beam defined in the input, consisting of 8 simulations, corresponding to the one where the geometry did not require an attenuator and the other 7 with attenuators of various thicknesses.

2.4. Estimation of air kerma for each exposure configuration and the HVL

Each of the output groups was processed in a Python algorithm (version 3.12) [20] responsible for condensing the relevant data for the next stage into just two files, which reduced the volume of files with data for exposures to each of the radiation beams to one-fourth.

Then, for each exposure to each beam, the mean energy, and the respective air kerma per photon were calculated using the conversion coefficients for air kerma per unit fluence, obtained once again through linear interpolation of values described in the literature for monoenergetic photons [17]. Exponential curve fittings were performed on the scatter of air kerma values per photon as functions of attenuator thicknesses, allowing estimates for the HVLs to be obtained. Using this number of points in the attenuation curve assures a good exponential fitting ($R^2 > 0.999$) and, consequently, a low statistical uncertainty in calculating

the HVL. Furthermore, it is coherent with the number of points proposed in the IAEA-TRS457 [21].

3. RESULTS AND DISCUSSIONS

All the following graphs were created using the Matplotlib library (version 3.8) [22] for Python (version 3.12) [20]. The graphs in Figs. 3 and 4 show the computationally estimated X-ray photon spectra for the interactions of monoenergetic electron beams of 30 keV, 60 keV, 80 keV, 100 keV, 200 keV, and 300 keV with the tungsten anode.

The characteristic emission lines of tungsten are evident. For the incident electron beams of 30 keV and 60 keV it is possible to identify the $M\alpha_1$ line and a peak corresponding to the superposition of the $L\alpha_1$, $L\alpha_2$, $L\beta_1$, $L\beta_2$, and $L\gamma_1$ lines. For the incident beam of 80 keV, it is also possible to identify the $K\alpha_1$ and $K\alpha_2$ lines. In the other X-ray spectra, the $K\beta_1$ line is still identifiable [23]. In all the spectra is evident the continuum emission band associated with the bremsstrahlung emission.

Figure 3 : Spectra of X-ray fields resulting from the interaction of electron beams of 30 keV, 60 keV, and 80 keV with a tungsten anode.

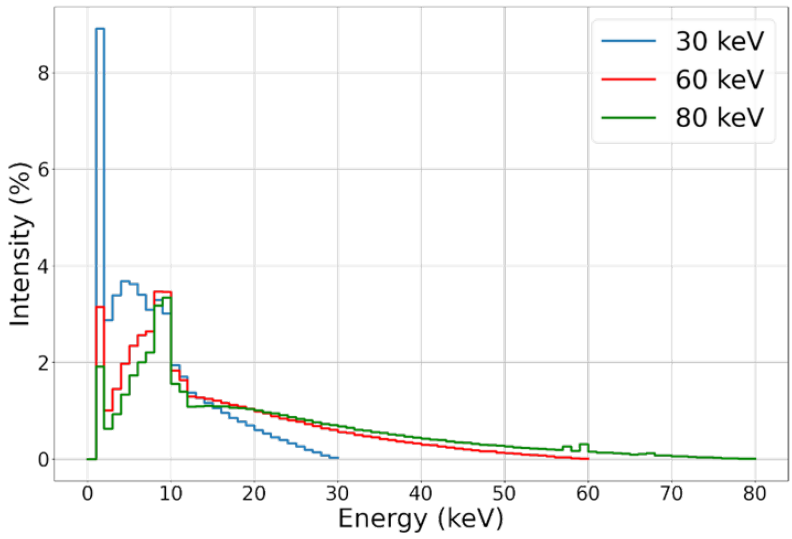

Figure 4 : Spectra of X-ray fields resulting from the interaction of electron beams of 100 keV, 200 keV, and 300 keV with a tungsten anode.

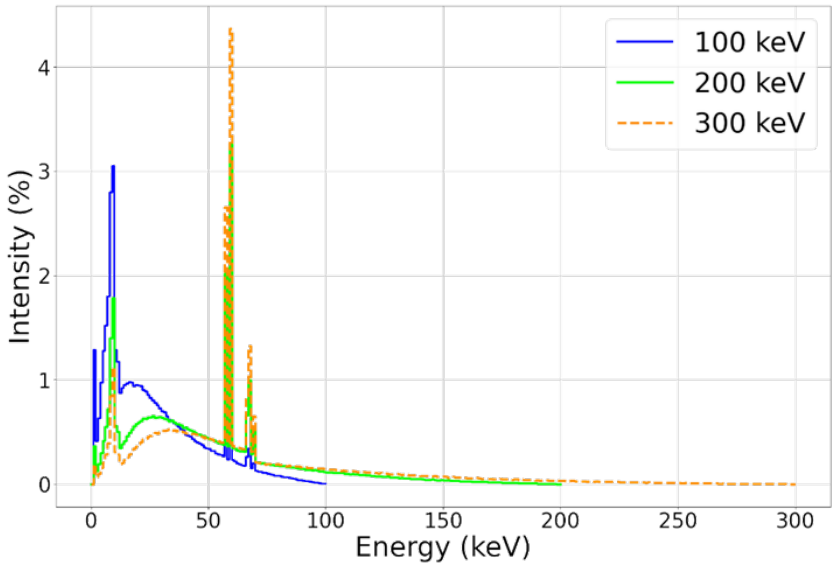

The graphs in Figs. 5 and 6, in turn, show the computationally estimated X-ray photon spectra, obtained from the filtrations of those shown in Figs. 3 and 4 according to the specifications of ISO 4037-1 [1] listed in Table 1, for the radiation beam qualities N30, N60, N80, N100, N200, and N300. A narrowing of the spectra around well-defined values for photon energy is observed due to the retention of low-energy photons by the filters.

The radiation beam quality N30 was computationally obtained due to the retention of photons with energies lower than 16 keV, and N60 is achieved through the retention of photons with energies less than 28 keV by the filters. For the quality N80, all photons with lower energy than 42 keV are retained, as well as those with energies lower than 56 keV for the radiation beam quality N100. Finally, to obtain the qualities N200 and N300, photons with energies lower than 121 keV and 179 keV, respectively, were retained by combining filters. All these spectra exhibit more fluctuations than the previous ones and are less precise than those provided by the PTB catalog [19], being not sufficiently to quantify the small fluence of lower energies photons than that expressed previously.

Figure 5 : Spectra of X-ray beam qualities N30, N60, and N80, according to the specifications of ISO 4037-1 [1].

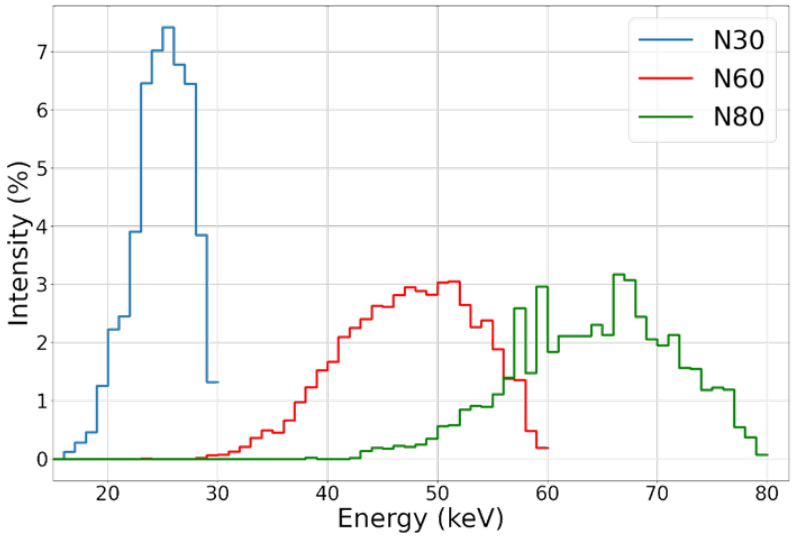

Figure 6 : Spectra of X-ray beam qualities N100, N200, and N300, according to the specifications of ISO 4037-1 [1].

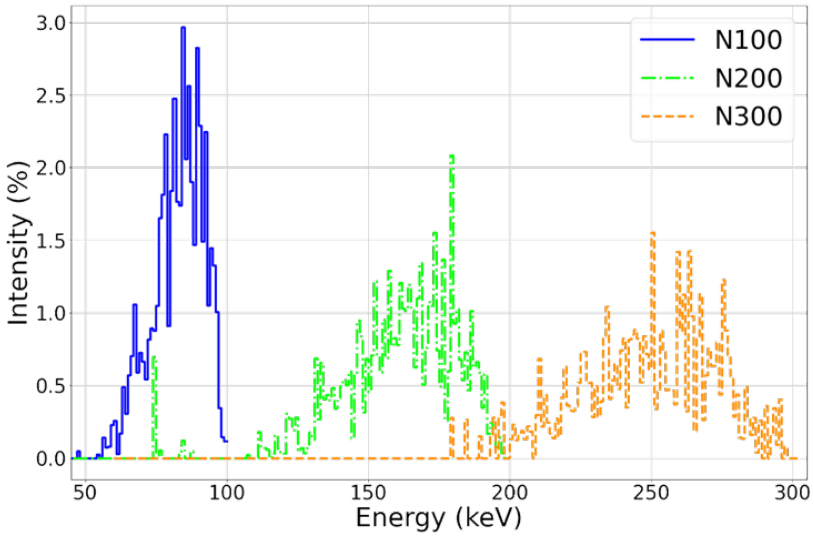

Table 2 shows the values described in the literature [19] for the mean energy photons $(\overline{E})$ in the radiation beam with the characteristics of the evaluated qualities, as well as the respective conversion coefficients for air kerma per unit fluence (K_a/Φ), compared with the values calculated from the spectra estimated by computational simulations. Additionally, the

respective statistical uncertainties are presented. Except for the estimated value for the conversion coefficient for the N30 quality beam, the other estimates show excellent agreement with the reference values.

Table 2 : Mean energy and conversion coefficients for air kerma per unit fluence associated with each radiation beam qualities, as related in the literature and computationally estimated, with respective statistical uncertainties.

Radiation beam quality	Reference ISO 4037-1 [1]		Computationally estimated X-ray spectra			
	$\overline{E}$ (keV)	K_a/Φ $(pGy.cm^2)$	$\overline{E}$ (keV)	K_a/Φ $(pGy.cm^2)$	r. error $\overline{E}$ (%)	r. error K_a/Φ (%)
N30	24.6	1.180	25±1	1.060±0.090	1.6	10.2
N60	47.9	0.365	47±1	0.346±0.009	1.9	5.2
N80	65.2	0.302	64±2	0.293±0.002	1.8	3.0
N100	83.3	0.325	83±4	0.320±0.010	0.4	1.5
N200	164.8	0.676	161±9	0.650±0.050	2.3	3.8
N300	248.4	1.110	250±20	1.100±0.100	0.6	0.9

Tables 3 and 4 present the relationships of air kerma per emitted photon for each source configuration and attenuator thickness, as well the respective statistical uncertainties, respectively, for the spectra that defined the probability density functions for photon energies obtained computationally, using PHITS, and extracted from the PTB spectrum catalog [19]. A more detailed evaluation of kerma for each configuration would require quantification in terms of tube current and exposure time, which is not trivial for the methodology adopted; however, the unit in which the magnitude is expressed does not affect the estimation of the HVL, which is the proposition of the work.

Table 3 : Relationships of air kerma per emitted photon for different beam qualities obtained computationally and different attenuator thicknesses, with respective statistical uncertainties.

	Kerma (aGy/photon)					
Beam attenuator (mmAl)	**N30**	**N60**	**N80**	**N100**	**N200**	**N300**
0.00	8.00±0.10	2.68±0.02	2.286±0.007	2.47± 0.02	5.13±0.04	8.70±0.07
0.25	6.90±0.10	2.60±0.02	2.250± 0.010	-	-	-
0.50	6.03±0.09	2.52±0.02	2.210± 0.010	2.40±0.02	5.04±0.04	8.57±0.07
1.00	4.61± 0.08	2.38±0.02	2.140±0.010	2.34±0.02	4.94±0.04	8.43±0.07
1.50	3.52±0.07	2.24±0.02	2.060±0.010	2.28±0.02	4.86±0.04	8.31±0.07
2.00	2.73±0.06	2.11±0.02	1.990±0.010	2.22±0.02	4.78±0.04	8.18±0.07
2.50	2.12±0.05	1.99±0.01	1.920±0.010	-	-	-
3.00	1.67±0.05	1.87±0.01	1.860±0.010	2.11±0.02	4.61±0.04	7.95±0.07
4.00	-	-	-	2.00±0.01	4.45±0.04	7.71±0.07
5.00	-	-	-	1.89±0.01	4.29±0.04	7.48±0.07

Table 4 : Relationships of air kerma per emitted photon for different beam qualities extracted from the PTB catalog [19] and different attenuator thicknesses, with respective statistical uncertainties.

	Kerma (aGy/photon)					
Beam attenuator (mmAl)	**N30**	**N60**	**N80**	**N100**	**N200**	**N300**
0.00	8.10±0.10	2.65±0.02	2.30±0.01	2.49±0.02	5.30±0.05	8.71±0.07
0.25	7.00±0.10	2.57±0.02	2.26±0.01	-	-	-
0.50	6.02±0.09	2.49±0.02	2.22±0.01	2.43±0.02	5.20±0.05	8.58±0.07
1.00	4.51±0.08	2.35±0.02	2.14±0.01	2.36±0.02	5.12±0.05	8.46±0.07
1.50	3.43±0.07	2.21±0.02	2.07±0.01	2.30±0.02	5.02±0.04	8.33±0.07
2.00	2.64±0.06	2.08±0.02	2.00±0.01	2.24±0.02	4.93±0.04	8.20±0.07
2.50	2.05±0.05	1.97±0.02	1.93±0.01	-	-	-
3.00	1.58±0.05	1.85±0.02	1.87±0.01	2.12±0.02	4.76±0.04	7.95±0.07
4.00	-	-	-	2.01±0.02	4.59±0.04	7.72±0.07
5.00	-	-	-	1.90±0.01	4.44±0.04	7.49±0.07

Table 5 shows the reference values of the HVL for each X-ray beam quality, as well as those obtained through beams with probability distributions for energies based on spectra estimated computationally using PHITS and those from the PTB catalog [19], including their respective statistical uncertainties. Except for the two estimated values of the HVL for the N30 quality beam, the others show good agreement with those described in the literature, and the magnitude of the relative error is similar regardless of whether PTB spectra are used [19] or those estimated computationally in the final stage of the method. Figure 7 graphically compares the three related values for each beam quality.

Table 5 : Reference values and estimates for the HVLs, with respective statistical uncertainties.

	Reference ISO 4037-1 [1]	**Computationally estimated X-ray spectra**		**PTB X-ray catalog spectrum[19]**	
Radiation beam quality	**HVL (mmAl)**	**HVL (mmAl)**	**r. error (%)**	**HVL (mmAl)**	**r. error (%)**
N30	1.16	1.31±0.01	12.9	1.25±0.02	7.8
N60	5.85	5.79±0.02	1.0	5.79±0.02	1.0
N80	9.90	9.96±0.04	0.6	9.97±0.04	0.7
N100	12.96	13.04±0.03	0.6	12.95±0.05	0.1
N200	19.40	19.45±0.07	0.3	19.44±0.05	0.2
N300	22.94	23.00±0.10	0.3	22.81±0.08	0.6

Figure 7 : Estimated thicknesses for the HVL associated with each beam quality compared to the values described in the literature [19].

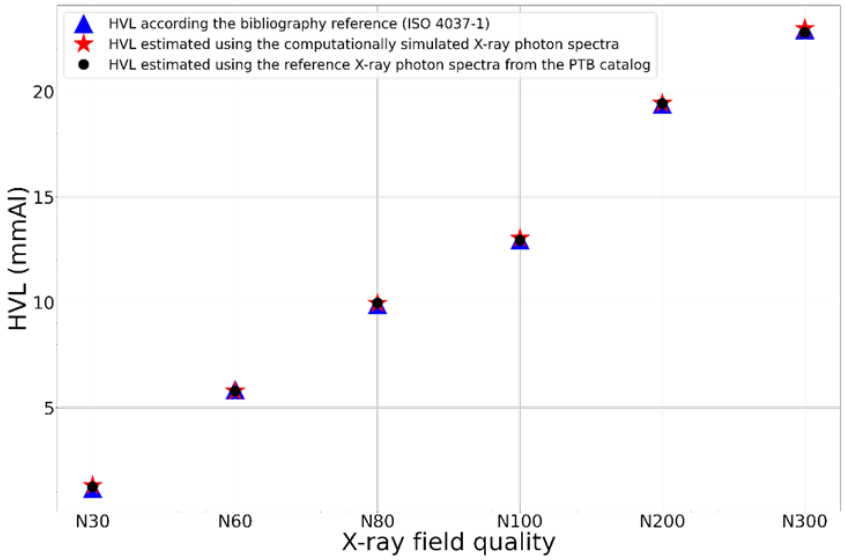

4. CONCLUSIONS

The present work proposes a methodology for determining the half-value layer associated with an X-ray beam quality through computational simulations using the Monte Carlo code PHITS. Although not the focus of the proposal, the methodology also allows for estimating spectra for different beam qualities, as well as the mean energy and the conversion coefficients for air kerma per unit fluence associated with them.

The results obtained show good agreement with the values described in the literature, demonstrating the potential of the code in simulating X-rays within the evaluated energy range. Surprisingly, using a computationally estimated spectrum obtained with PHITS for the incident radiation beam, using a relatively simple method, did not significantly affect the relative errors of the results compared to using a reference spectrum from the PTB catalog.

The main limitation of the study lies in the difficulty of quantifying the air kerma associated with beam quality through tube current and exposure time, which constitutes a potential research objective. Furthermore, it is anticipated that efforts will be made to

improve the methodology to more thoroughly assess the uncertainties associated with the estimates, not only the statistical ones but, especially, those inherent to the geometry, calculation methodology and the conversion coefficients for air kerma per unit fluence. This could potentially help understand the discrepancy in the estimates of quantities for the N30 beam quality compared to the reference values specified in ISO 4037-1.

Finally, the developed methodology proved to be efficient for the proposed application and opens perspectives for further explorations to evaluate other radiological quantities associated with beam qualities.

ACKNOWLEDGMENT

R.E. Soares is grateful to CNPq (Conselho Nacional de Desenvolvimento Científico e Tecnológico) for the scholarship (undergraduate scientific grant PIBIC/CDTN/CNPq). M.A.S. Lacerda is grateful for the financial support provided by FAPEMIG (Fundação de Amparo à Pesquisa do Estado de Minas Gerais-Project: Universal Proc. APQ-01018-21).

We appreciate the generosity of our colleagues and Santos V.C.P., who conducted simulations on their personal computers to generate new results and enhance those previously utilized in this work.

FUNDING

R.E Soares have received scholarship from CNPq (Conselho Nacional de Desenvolvimento Científico e Tecnológico) through PIBIC Programa Institucional de Bolsas de Iniciação Científica (CDTN/CNPq). M.A.S. Lacerda receive financial support provided by FAPEMIG (Fundação de Amparo à Pesquisa do Estado de Minas Gerais-Project: Universal Proc. APQ-01018-21). This work is part of the Brazilian Institute of

Science and Technology for Nuclear Instrumentation and Applications to Industry and Health (INCT/INAIS), CNPq project 406303/2022-3.

CONFLICT OF INTEREST

All authors declare that they have no conflicts of interest.

REFERENCES

[1] International Organization for Standardization. (2019). Radiological protection—X and gamma reference radiation for calibrating dosemeters and doserate meters and for determining their response as a function of photon energy—Part 1: Radiation characteristics and production methods. ISO, 4037–1.

[2] JOHNS, H. E.; CUNNINGHAM, J. R. **The physics of radiology**. 4th ed ed. Springfield, Ill., U.S.A: Charles C. Thomas, 1983.

[3] BUSHBERG, J. T. (ED.). **The essential physics of medical imaging**. 3rd ed ed. Philadelphia: Wolters Kluwer Health/Lippincott Williams & Wilkins, 2012.

[4] LACERDA, M. A. DE S.; SILVA, T. A. DA; OLIVEIRA, A. H. DE. Influência da metodologia de avaliação da camada semi-redutora em radiologia diagnóstica. **Radiologia Brasileira**, v. 40, p. 331–336, 2007.

[5] ED, T. Determination of half-value layer. Am J Roentgenol, v. 84, n. 4, p. 729–740, 1960.

[6] ICRU. Physical Aspects of Irradiation. Washington, **D.C.: International Commission on Radiation Units and Measurements**, 1962.

[7] SILVA, F. S. G. DA. Aplicação de método Monte Carlo para cálculos de dose em folículos tiroideanos. Recife, PE: Universidade Federal Rural de Pernambuco, 2008.

[8] ROGERS, D. Fifty years of Monte Carlo simulations for medical physics. **Physics in Medicine & Biology**, v. 51, n. 13, p. R287, 2006.

[9] AGOSTINELLI, S. et al. Geant4—a simulation toolkit. **Nuclear Instruments and Methods in Physics Research Section A: Accelerators, Spectrometers, Detectors and Associated Equipment**, v. 506, n. 3, p. 250–303, 2003.

[10] FERRARI, A. et al. FLUKA: a multi-particle transport code. CERN-2005-10, 2005.

[11] BEATTIE, K. et al. TOPAS version 3.9, 2022. Disponível em: <https://topas.readthedocs.io/en/latest/> .

[12] KULESZA, J. A. et al. MCNP® code version 6.3. 0 theory & user manual. [s.l.] Los Alamos National Lab.(LANL), Los Alamos, NM (United States), 2022.

[13] SALVAT, F.; FERNÁNDEZ-VAREA, J. M.; SEMPAU, J. PENELOPE-2006: A code system for Monte Carlo simulation of electron and photon transport. **Nuclear Instruments and Methods in Physics Research Section B: Beam Interactions with Materials and Atoms**, v. 265, n. 3, p. 509–525, 2007.

[14] SATO, T. et al. Recent improvements of the particle and heavy ion transport code system–PHITS version 3.33. **Journal of Nuclear Science and Technology**, p. 1–9, 2023.

[15] CAMPILLO-RIVERA, G. E. et al. X-ray spectra and gamma factors from 70 to 120 kV X-ray tube voltages. **Radiation Physics and Chemistry**, v. 184, p. 109437, jul. 2021.

[16] DE JESUS TEIXEIRA, G. et al. Facilidades de códigos de Monte Carlo para obter CSR. **Brazilian Journal of Radiation Sciences**, v. 7, n. 3B (Suppl.), 2019.

[17] ICRU, M. ICRU Report 57-Conversion Coefficients for Use in Radiological Protection Against External Radiation. 1997.

[18] R CORE TEAM. R: A Language and Environment for Statistical Computing. R Foundation for Statistical Computing, 2024. Disponível em: <https://www.r-project.org/>.

[19] ANKERHOLD, U. Catalogue of X-ray spectra and their characteristic data: ISO and DIN radiation qualities, therapy and diagnostic radiation qualities, unfiltered X-ray spectra. Bremerhaven: Wirtschaftsverl. NW, Verl. für Neue Wiss, 2000.

[20] PYTHON SOFTWARE FOUNDATION. Python 3.12 Documentation. Python Software Foundation, 2024.

[21] INTERNATIONAL ATOMIC ENERGY AGENCY. Dosimetry in Diagnostic Radiology: An International Code of Practice. IAEA Technical Reports Series No. 457. Vienna: IAEA, 2007. 247 p.

[22] MATPLOTLIB DEVELOPMENT TEAM. Matplotlib: Visualization with Python. Matplotlib Development Team, 2023. Disponível em: <https://matplotlib.org/>.

[23] BOOKLET, X-Ray Data. X-ray Data Booklet. Laboratory, Univ. California, 2001. Table 1-2.

LICENSE